Engineering Structures 275 (2023) 115152

Contents lists available at ScienceDirect

Engineering Structures

journal homepage: www.elsevier.com/locate/engstruct

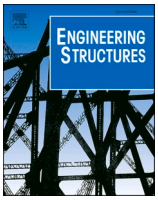

A novel mechanism - smart morphing façade system - to mitigate wind-induced vibration of tall buildings

Fangwei Hou [a], Partha P. Sarkar [a,*], Alice Alipour [b]

[a] Department of Aerospace Engineering, Iowa State University, 537, Bissell Road, Ames, IA 50011, USA
[b] Department of Civil, Construction and Env. Engineering, Iowa State University, Ames, IA 50011, USA

ARTICLE INFO

Keywords:
Tall-building response
Wind-induced vibration
Morphing-building façade
Aeroelastic model test
CAARC tall-building model
Wind tunnel testing
Vibration mitigation

ABSTRACT

Wind-induced vibration plays a significant role in the design of tall buildings, primarily due to serviceability requirements for occupant comfort and structural safety. As a result, several approaches have been developed to address this concern. This paper describes a novel control mechanism, a smart-morphing-façade (*Smorphacade*) system, using the concept of an aerodynamically modified building façade to mitigate wind-induced vibration of tall buildings. Compared to a fixed-façade system, since a *Smorphacade* can be dynamically modified in real time based on rapidly-changing wind speed and wind direction during a windstorm, it can be further developed into an active control system. The *Smorphacade* is comprised of a set of circular ducts embedded in a flat plate and arranged in a matrix formation that is fixed on the original façade but with a gap between the two facades. Each circular-shaped duct is comprised of two parts, a fixed base with alternate open and closed surfaces shaped like a fan-blade and a rotating part similar in shape like the fixed one but placed inside the fixed one and capable of rotation by a protruding fin. By rotating the fin, the porosity of the duct and the fin inclination angle can be simultaneously changed, enabling flow control through the duct. The performance of a *Smorphacade* system in different configurations was studied using the CAARC standard tall-building model under atmospheric boundary layer wind; its effectiveness in reducing building response was examined by comparing the results of a building with a *Smorphacade* system to those from one without it. It was found that the effectiveness of the *Smorphacade* system in reducing the average combined vibration among all three directions (2 transverse and 1 torsional) varied between 16.7 and 18.6%, with a maximum reduction of 32% and 59.7% in across-wind direction and torsional direction, respectively, depending on factors such as *Smorphacade* configuration, wind speed, and angle of attack.

1. Introduction

As building designs become taller and more slender, they also become more flexible and subject to high winds that significantly increase their flexure. If left uncontrolled, excessive wind-induced building vibration can cause serious problems. For example, large oscillatory displacements may require reducing the elevator speed during strong winds, or may damage brittle secondary elements such as partitioning, glazing, and the building facade. Accumulation over many cycles of large-amplitude vibration can also result in fatigue failure. Wind-induced movement can lead to two other significant problems: (1) audible cracking resulting from large relative motion between building parts as the building deflects [1,2], and (2) a perception of movement arising from large accelerations, most prevalent at higher levels, leading to motion sickness and sopite syndrome [3–9]. Because of the impact of wind-induced vibration on serviceability of tall buildings, numerous studies have been carried out to control such vibration [6,7,8,10,11]. Since tall buildings are like bluff bodies whose aerodynamic behavior is influenced by their shapes, wind loads on tall buildings can be reduced through aerodynamic modification of their outer surfaces or their facades. It has been shown that modifying the exterior shape of a tall building can result in reduction of wind load in the across-wind direction along the building height, and the effectiveness of shape modification in reduction of wind loads on tall buildings has been widely investigated. Shapes considered to be effective in this regard include polygon or Y-type sections and corners for sectional shape (horizontally), taper, setback, and openings for building shape (vertically) [12–13]. Tanaka et al. [16] performed a series of wind-tunnel tests to evaluate

* Corresponding author.
E-mail address: ppsarkar@iastate.edu (P.P. Sarkar).

https://doi.org/10.1016/j.engstruct.2022.115152
Received 20 July 2021; Received in revised form 11 September 2022; Accepted 15 October 2022
Available online 16 November 2022

various aerodynamic modifications that could reduce wind loads on tall buildings. Along with experimental approaches, numerical simulation techniques, e.g., Computational Fluid Dynamics (CFD), have also been adopted for studying the influence of building shape on wind loads [17–18]. Both numerical and experimental studies have revealed that modification of exterior shape can significantly reduce wind loads on tall buildings; the significance of such aerodynamic modification is dependent on both the type of modification and the wind direction. Nevertheless, tall buildings have traditionally been designed with a specific aerodynamic shape derived from crude estimates of average flow conditions under atmospheric boundary-layer winds, and such design can produce building shapes not necessarily effective under non-synoptic winds such as hurricanes, thunderstorms, tornadoes, and microbursts with highly-transient characteristics in terms of intensity, fluctuations (turbulence), and direction. Furthermore, as urban areas become more populated, the need to construct more tall buildings is intensified, leading to possibilities of interferences introduced by adjacent buildings that were not accounted for during a building's design, underlining the need for design that can properly control building-façade behavior subjected to variable and unpredictable airflows.

A building envelope can play a key role in attaining building energy efficiency and satisfactory indoor comfort, with suitable ventilation being an important contribution. In a special category of facades, double-skin facades (DSF), where a secondary exterior façade is added to a building envelope, a pressure difference induced by wind can drive airstreams through the cavity between the inner and outer layers of the DSF, resulting in reduced building temperature with no added energy cost. Since wind can play an important role in the DSF performance of buildings, numerous studies investigating the effect of wind on DSFs have been conducted. Van Moeseke et al. [21] measured the pressure coefficient distribution on buildings both with and without a façade, particularly studying effect of two parameters, wind incidence and environment density. Lou et al. [22] used wind-tunnel tests to obtain the wind-pressure distribution on double-skin facades for different DSF layouts, air corridor widths and incident wind angles, and a numerical method, a so-called zonal approach, was employed to calculate wind-induced inner-gap pressures on the DSF. Effectiveness was validated by comparing the numerical results with those from experimental testing. In addition to contributing to ventilation, a building façade can also be used for energy harvesting by placing wind turbines inside the façade cavity to harvest energy from the air that flows through the openings. Hassanli et al. [23] proposed a DSF with strategic openings based on the pressure field around the building to enhance wind flow for energy harvesting. The characteristics of wind flow inside the DSF cavity were studied using both CFD simulation and wind tunnel test, and it was found that the façade can effectively change the wind flow in terms of mean wind speed and turbulence intensity. Hassanli et al. [24] additionally examined the effect of modifications involving corridors, recessed regions, and curved walls on flow characteristics of the building and the original DSF. They found that appropriate modifications can enhance the wind flow, with the extent of the enhancement depending both on the wind inclination and the type of modification.

Both ventilation and energy-harvesting are examples of the capability of a façade to modify wind-flow characteristics around buildings while giving it a potential to be used for wind-induced vibration mitigation. In fact, there have been many studies assessing the possibility of using passive forms of façades to reduce wind loads on buildings. Silva and Gomes [25] used wind-tunnel tests to measure pressure distribution inside the DSF gap, and various layouts for building DSFs that could affect wind pressure were analyzed. The experimental data indicated that wall-pressure distribution in buildings with DSF was distinct from that of an unsheltered building. Hu et al. [26], studying the effects of a DSF system on wind-induced responses of a tall building, found that a façade with/without openings has a negligible impact on along-wind response, while a façade with openings can significantly decrease across-wind response compared to that of bare buildings. They therefore concluded that along with improving indoor environment and reducing energy use, DSF can be utilized to mitigate wind-induced vibration of buildings. Fu and Johnson [27] proposed external shading fins, as attached to the façade of a tall building, to act as distributed mass damper system to control building movements by dissipating energy with these dampers during strong motions due to wind or earthquake, while helping to adjust the amount of external sunlight getting inside the building for reducing energy consumption. Yuan et al. [28] systematically investigated the effect on wind pressures of various arrangements of façade appurtenances, using horizontal thin splitter plates attached to the façades of high-rise buildings. Configurations classified in terms of horizontal gap-distance ratios, vertical separation-distance ratios, and extensional depth ratios of the thin plates were investigated, and it was found that the peak-pressure coefficient of a building can be reduced by as much as 42 %. In a similar study, Yang et al. [29] carried out a series of wind-tunnel experiments to evaluate the influence of vertical splitter plates attached to the building's façade, and the experimental results revealed that vertical plates could significantly reduce mean and fluctuating pressure, along- and across-wind loads, and base moment for certain configurations. Pomaranzi et al. [30] reported measurement of peak pressures on the inner skin of a porous DSF system, assessed aerodynamic effects of porosity on the pressure distribution on the inner façade of the DSF system, and showed that both positive and negative peak pressures can be reduced by up to 40 % in contrast to a standard façade system. Jafari and Alipour [31,32] provided a complete review of the existing opportunties to use the passive aerodynamic shape modification of the building and DSF to reduce the wind load effects.

Despite encouraging results with respect to reducing wind loads on buildings, the aforementioned studies were on passive or static façades without the ability to change with wind speed or direction, and such passive façade systems cannot be very effective under circumstances where the wind events are highly transient. This shortcoming justifies the development of smart morphing façade modules capable of responding to changes in wind regime and real-time dynamic modification of the aerodynamic shape of the building surface based on rapidly-changing wind speed and wind direction in windstorms such as thunderstorms, downbursts, and tornadoes, to alleviate wind-induced vibration. To this end, this paper proposes a smart-morphing façade (dubbed as *Smorphacade*) system that can actively modify the aerodynamics of tall buildings to alleviate wind-induced vibration. Abdelaziz et al. [33] developed the computational control concept and Jafari and Alipour [32] conducted the respective CFD analyses to justify the concept.. The proposed *Smorphacade* system is comprised of a set of circular ducts embedded in a flat plate and arranged in a matrix formation fixed on the original façade, with a gap between the two facades. Each circular-shaped duct comprises of two parts, a fixed base with alternate open and closed surfaces shaped like fan blades, and a rotating part placed inside the fixed one and similar in shape that can be rotated by a protruding fin. By rotating the fin, the porosity of the duct as well as the fin inclination angle can be simultaneously changed, enabling flow control through the duct. It was found in the literature that both the porosity of the façade and the configuration of splitter plates on the façade can significantly impact wind loads on buildings. To evaluate their performance in the mitigation of wind-induced vibration, the *Smorphacade* panels were attached to an aeroelastic tall building model. Three critical angles of attack were tested and the acceleration responses of the aeroelastic model were obtained. The proposed *Smorphacade* system can be further used to develop an active control system when incorporated with strategically-positioned pressure/velocity/acceleration sensors, with measurements from those sensors utilized as inputs to a control system that would manipulate the smart-morphing façade in a coordinated fashion to reduce or eliminate flow-induced effects that could possibly result in excessive vibration.

This paper is organized as follows: Section 2 is a description of the proposed *Smorphacade* system and the aeroelastic tall building model. Section 3 details wind-tunnel tests used to assess the effectiveness of the

proposed system. Section 4 presents and discusses the experimental results. Finally, Section 5 gives a summary of the results.

2. Description of the Smart-Morphing-Façade system

2.1. Aeroelastic tall building model

The performance of the *Smorphacade* was studied on the CAARC (Commonwealth Advisory Aeronautical Research Council Coordinators) standard tall-building model under atmospheric boundary layer (ABL) winds, and its effectiveness with respect to reducing the building response was examined by comparing the results for the building that implemented the *Smorphacade* system with those for the one without it. The CAARC standard tall building model is an aeroelastic model of a tall building with a rectangular cross section that was proposed by a group of scholars to coordinate benchmark studies comparing buffeting response of a tall building model subjected to well-defined simulated wind from various wind tunnels [34]. The aeroelastic model of the building developed for this study was fabricated with a geometric scale of 1:175. It had a rectangular cross section with dimensions $B = 0.261$ m, $D = 0.174$ m, and height $H = 1.05$ m, resulting in aspect ratios $B/D = 1.5$ and $H/D = 6$. The aeroelastic model was built with four solid steel columns connected to the ground to offer structural stiffness. The lumped mass of the tall building was modeled using five rectangular Plexiglass plates attached to the four columns at different heights using nuts (hence a 15 degree of freedom or 15 DOF system). Four panels were attached to each of the five Plexiglass plates representing the 4 floors and the roof of the building to cover the model sides and represent the building facade, and a gap of 2 mm was established between the adjacent panels along the model height to ensure free lateral and torsional motion of the model when subjected to wind. This arrangement allowed for aeroelastic model vibration in across-wind, along-wind, and torsional directions. Further details of this aeroelastic model can be found in [35].

In the CAARC building with the added *Smorphacade*, the panel dimensions were matched with those of the wall panels of the aeroelastic model, with the *Smorphacade* acting as a secondary exterior façade (resembling a DSF). The sizing of the *Smorphacade* panels were: 261 mm × 207 mm (8 panels), 261 mm × 103 mm (2 panels), 174 mm × 207 mm (8 panels) and 174 mm × 103 mm (2 panels). Fig. 1 shows the developed primary standard CAARC standard aeroelastic building both with and without the *Smorphacade*.

2.2. The Smart-Morphing Façade (Smorphacade) system

The *Smorphacade* panels were attached to the original panels of the aeroelastic model using thin magnetic strips along their edges. It was comprised of a set of circular ducts embedded in a 6-mm thick flat plate and arranged in a matrix formation fixed on the original façade while maintaining a 2-mm gap between the two facades. Each circular-shaped duct was comprised of two parts, a fixed base with alternate open and closed fan-blade shaped surfaces (referred to here as stationary-fan) and a rotating part placed inside the fixed one and similar in shape (referred to here as rotating-fan) capable of rotation about its center by a protruding fin (Fig. 2). By rotating the fin, because of the overlap between the two sets of blades the porosity of the duct and the fin inclination angle can be simultaneously changed, enabling the control of flow through the duct.

Once the rotating-fan is in the desired position with respect to the stationary-one, its position can be fixed by tightening a screw that runs through the center of each circular duct. The stationary fan has a diameter of 42 mm. Since there are 20 ducts on the 261 mm × 207 mm panel, 10 ducts on the 261 mm × 103 mm panel, 12 ducts on the 174 mm × 207 mm panel, and 6 ducts on the 174 mm × 103 mm panel, therefore, the *Smorphacade* fan system has 288 ducts in total. The stationary-fan units shown in Fig. 2a have two blades, each with a subtended angle of 36°, and two openings, each with a subtended angle of 144°, with a hole at the center to provide room for the screw. The rotating-fan has a fin that sticks out of the panel (like a knob) that can move with the fan when it rotates. The length of the fin exceeds the diameter of the duct to establish better continuity between the neighboring ducts and therefore throughout the entire panel system. The fin

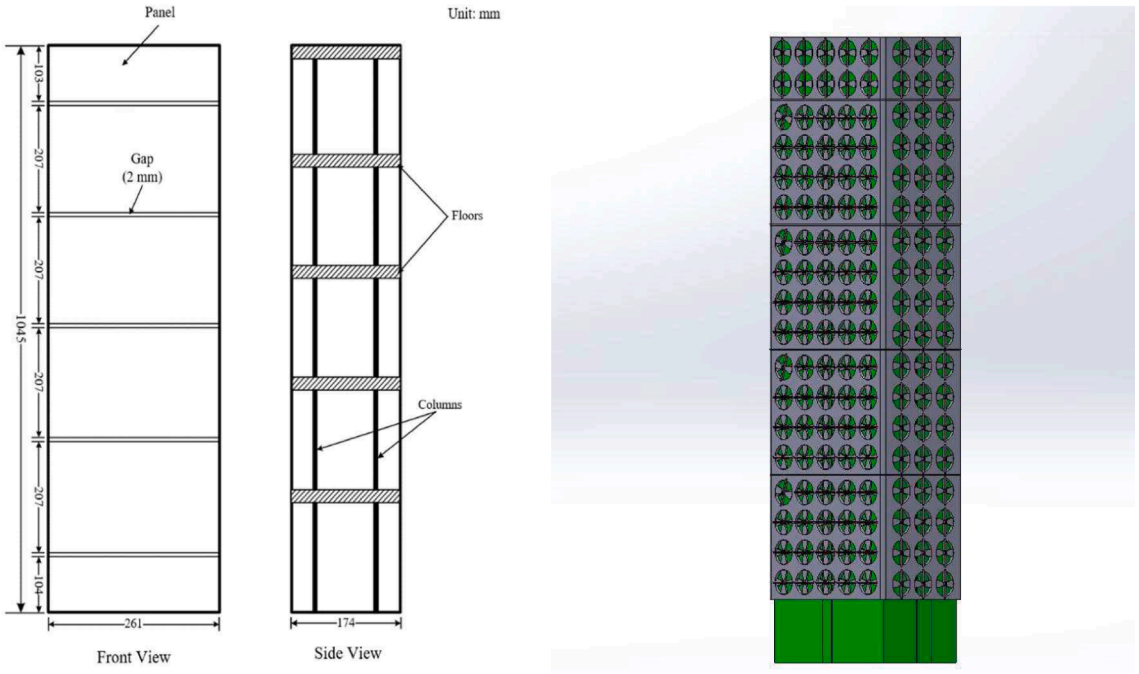

Fig. 1. Schematics of the: (a) CAARC Building Model, and (b) CAARC Building Model with *Smorphacade* System.

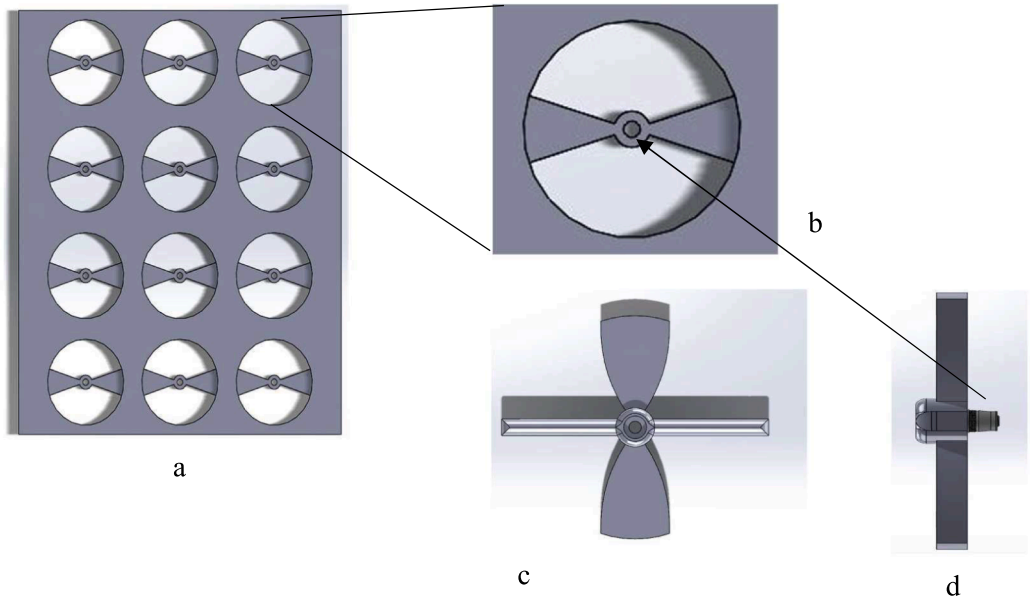

Fig. 2. Schematic of the *Smorphacade*: a) a typical panel with stationary-fan units, b) a stationary-fan unit (expanded view), c) rotating-fan unit with fin (front view), and (d) rotating-fan unit with fin (side view).

protrusion in the circular duct units over the facade was 10 mm for the top 3 panels used to cover each wall over a height of 517 mm (1x103 + 2 x207) or 0.492H, while the fin protrusion in the circular duct units over the facade was 2 mm for the bottom 2 panels on each wall over a height of 414 mm (2x207) or 0.394H. For aerodynamic modification on the façade, the fin angle in each unit of the façade system can be independently changed. The porosity (ratio of open area to total area of each duct) changes as a function of the position of the fin, and such variable porosity and fin orientation of each duct provides a mechanism for modifying the flow impinging on the building surface. The proposed system is expected to reduce wind-induced pressures on the building in a manner similar to the DSF system with a gap between the two façades mentioned earlier. This is similar to pressure reduction behind a screen, except now the screen porosity can be dynamically changed by controlling the fin positions in real time. The fins were conceived to have multiple functions, including providing a rough surface to make the flow turbulent by dispersing it, directing the flow in certain directions along the surface of the facade, and providing aerodynamic damping in a direction normal to the surface of the fin much like a flat plate does.

The *Smorphacade* runs along the height of the building model except for the bottom panel, because it was assumed that the influence of the wind flow around the bottom of a building on the building response would be negligible. Fig. 1b is a schematic diagram of the *Smorphacade panels* mounted on the aeroelastic model.

2.3. Aesthetics and practicality of the Smorphacade system

Aesthetics and practicality of the proposed *Smorphacade* System need to be put here in context. Both aesthetics of a building and functionality of its façade for providing an outside view for the building occupants are important. "Origami-shaped facade tsuch as those used in Al-Bahr Tower building in Abu Dhabi have been shown to have aesthetic as well as energy saving applications. In a collaborative design process with architects, structural designers, and wind engineers the morphing facades could be designed to not only be aethetically pleasing but also perform as a means to enhance the aerodynamic performance of the building. The functionality of these façades to provide an outside view can be achieved by making them with transparent materials, or if these façades indeed block the view, then the outside view can be projected on the inside surface of the external walls of the building by external cameras connected by numerous fiberoptic cables. It should also be mentioned that in the context of wind applicaitons, it is not expected that the facades need to be activated all the time. They only activate (and initiate morphing) when particular wind regimes are observed at the site. The concept of using *Smorphacade* on tall buildings with the goal of decreasing wind load effects and vibration is new but the concept of using dynamic (or adaptive) façade (open and close configurations) is already in use in a few existing buildings like the Al-Bahr Tower Building in Abu Dhabi for the purpose of energy savings and glare control. This study demonstrates that the S*morphaçade* can also serve the purpose of vibration control, as evidenced from the results presented here, and if matched along with energy conservation, the justification for such systems will be achieved. Compared to TMD or TML that are designed for a single band width (and normally the dominant natural frequency of the building), the *Smorphacades* have the added benefit of being able to cover the potential changes in wind regime (either due to climate change or change in neighboring buildings configuration) as well as higher mode effects. Maintenance of the distributed *smorphaçade* system will be expensive but if it is paired with their energy saving capacity (similar to existing adaptive facades). then it can offset or eliminate that added costs. Furthermore, becaue of distributed nature of the morphing facades, the failure of one module would not have major impact on the performance of the system, a fact that could not be said in the case of TMD or TML. . A detailed cost-benefit analysis of the *smorphaçade* system is needed before it can be made practical.

3. Experimental tests

To test its effectiveness in reducing the wind-induced response, wind-tunnel static tests on section models and dynamic tests on an aeroelastic model, as described earlier, both with and without the *Smorphacade* system, were conducted. These tests were carried out in the ABL (atmospheric boundary layer) test section of the Aerodynamic and Atmospheric Boundary Layer (AABL) Wind and Gust Tunnel located in the Wind Simulation and Testing Laboratory (WiST Lab) of the Department of Aerospace Engineering at Iowa State University. This wind tunnel has two test sections, an aerodynamic test section of 2.44 m (8.0 ft.) width × 1.83 m (6.0 ft.) height with a maximum wind speed capability of 53 m/s (173.9 ft/s), and an ABL test section of 2.44 m (8.0 ft.) width × 2.21 m (7.25 ft.) height with a maximum wind speed

(average) capability of 40 m/s (131 ft/s).

To measure the wind-induced vibration of the wind-tunnel model, six unidirectional accelerometers (PCB Model 352C65) were attached to the inside surface of the wall panels of the aeroelastic model at two different levels, namely, roof-height (H) and mid-height ($0.55H$). The accelerometers used in the tests have a capability of $\pm$ 491 m/s^2 ($\pm$50 g peak) and a sensitivity of 10.2 mV/m/s^2. When connected to NI 9205 Data Acquisition System that offers 16-bits resolution over a range of $\pm$ 10 V, the accelerometer resolution was 0.015 m/s^2. Mass eccentricity caused by accelerometer mass (2 g each) was eliminated by attaching nuts with masses identical to that of the accelerometers to the opposite wall panels of the aeroelastic model. The accelerometer locations, the definition of angle of attack (AOA), and coordinates (x_b, y_b, α) for the aeroelastic model are shown in Fig. 3.

Wind-induced vibration of the building model for three critical wind angles of attack, AOA (angle of attack) = 0° (normal to the short side), 34° (along-diagonal) and 90° (normal to the broad side), were tested. At each AOA, the acceleration of the model was measured at different wind speeds such that the relationship between wind-induced vibration and reduced velocity ($RV = \frac{U_H}{n_1 D_c}$, where U_H is mean wind speed at building roof height, n_1 is the first natural frequency of the model, $D_c = \sqrt{BD} =$ 0.213 m is a characteristic length of the building floor plan area) could be determined. For each measurement, the accelerations in x_b- and y_b-direction can be obtained using:

$$a_{xb,\text{roof}} = A_3,\ a_{xb,\text{mid}} = A_6,\ a_{yb,\text{roof}} = A_1,\ a_{yb,\text{mid}} = A_4 \tag{1}$$

The α-direction acceleration can be calculated using:

$$a_{\alpha,roof} = \frac{A_2 - A_3}{R},\ a_{\alpha,mid} = \frac{A_5 - A_6}{R} \tag{2}$$

where A_1 through A_6 denote accelerations measured by accelerometer #1 through 6, R is the distance between the accelerometers (#2 at the roof height, #5 at mid-height) and the center of the cross section, as shown in Fig. 3.

The mass of the aeroelastic model would increase because of the attachment of *Smorphacade* panels to it. To eliminate such an effect of increase in mass on the dynamic response of the model with the *Smorphacade*, plain Plexiglass panels (called dummy panels) of mass equal to the *Smorphacade* panels were attached to the original model (base model). By comparing the results of the aeroelastic model equipped with *Smorphacade* to those obtained with *dummy* panels, the effectiveness of Smorphacade in the mitigation of wind-induced vibration of tall buildings was evaluated. Fig. 6 shows the wind tunnel test setup of the aeroelastic model equipped both with *Smorphacade* panels and with *dummy* panels.

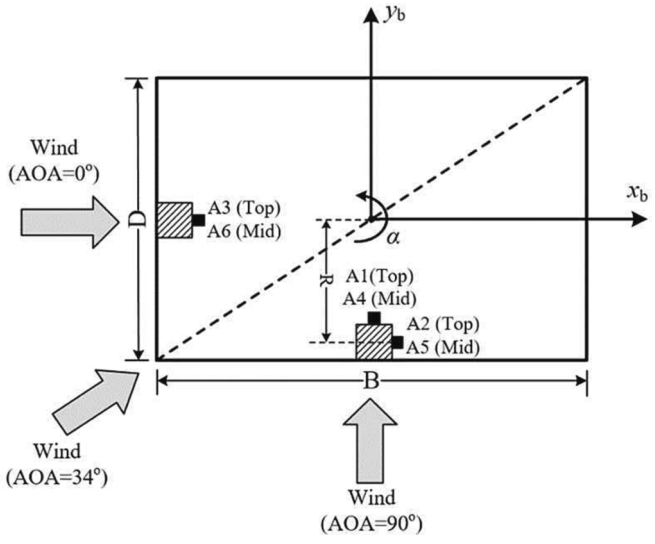

Fig. 3. Locations of accelerometers and definition of AOA and building coordinates.

A total of ten cases, configured with different fin angles and distributions on the four walls of the building model (over the top half of the building over 0.492H height), were tested. The fin angles could be positioned at 0, 45, 70 and 90°, where 0° is the horizontal position and 90° is the vertical position. The porosity of the *Smorphacade* system, dependent on the fin position, was determined for each configuration. The porosity, defined as the ratio of the porous area to the total area of each *Smorphacade* panel, was varied between 54.7 %, 64 % and 76.4 %. The test cases and their corresponding fin angles and porosities are summarized in Table 1, and the wall face number is defined in Fig. 4. Fig. 5 shows two different configurations of *Smorphacades* mounted on the aeroelastic model while Fig. 6 shows the setup for the boundary-

Table 1
The configuration of *Smorphacade* panels.

Conf./ Case No.		Face #1	Face #2	Face #3	Face #4
1	Fins				
	Inclination angle	45°	45°	45°	45°
	Porosity	54.7 %	54.7 %	54.7 %	54.7 %
2	Fins				
	Inclination angle	90°	90°	90°	90°
	Porosity	76.4 %	76.4 %	76.4 %	76.4 %
3	Fins				
	Inclination angle	0°	0°	0°	0°
	Porosity	54.7 %	54.7 %	54.7 %	54.7 %
4	Fins				
	Inclination angle	90°	45°	90°	45°
	Porosity	76.4 %	54.7 %	76.4 %	54.7 %
5	Fins				
	Inclination angle	45°	90°	45°	90°
	Porosity	54.7 %	76.4 %	54.7 %	76.4 %
6	Fins				
	Inclination angle	0°	45°	0°	45°
	Porosity	54.7 %	54.7 %	54.7 %	54.7 %
7	Fins				
	Inclination angle	45°	0°	45°	0°
	Porosity	54.7 %	54.7 %	54.7 %	54.7 %
8	Fins				
	Inclination angle	0°	90°	0°	90°
	Porosity	54.7 %	76.4 %	54.7 %	76.4 %
9	Fins				
	Inclination angle	0°	0°	90°	0°
	Porosity	76.4 %	54.7 %	76.4 %	54.7 %
10	Fins (Inclination = 70°)				
	Inclination angle	70°	70°	70°	70°
	Porosity	64 %	64 %	64 %	64 %

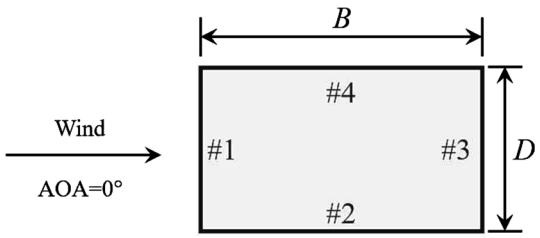

Fig. 4. The definition of wall face numbers.

layer simulation with spires and roughness blocks in the ISU's AABL Wind and Gust Tunnel, with the aeroelastic model of a tall-building model with and without the *Smorphacade* mounted on the turntable.

4. Results

4.1. Wind profile

The wind-tunnel model was tested in an atmospheric boundary layer (ABL) flow corresponding to a dense suburban terrain, an expected condition for tall buildings in urban regions. The aeroelastic model was fixed to a turntable in the ABL test section of the AABL Wind and Gust Tunnel at ISU, and ABL flow corresponding to a suburban terrain was generated \ using a combination of spires and wooden blocks placed on the wind tunnel floor in front of the aeroelastic model. While the spires were fixed at the exit of the contraction section or at the entrance of the test section of the wind tunnel, wooden blocks of different sizes and spacing were carefully arranged in a certain sequence and laid on the wind tunnel floor over a 50-meter-long fetch to generate the desired ABL

(a) Configuration No. 1

(b) Configuration No. 3

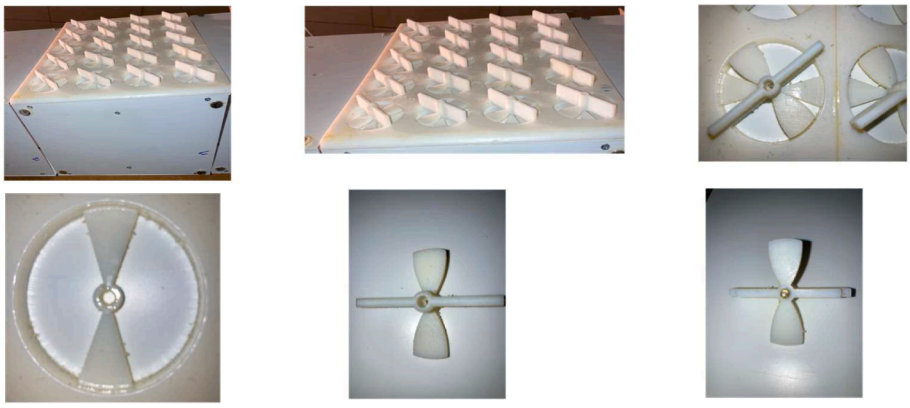

(c) (clockwise from top left): a typical panel mounted on one wall of the model, the perpendicular wall is exposed to show magnetic buttons used for mount; closeup view of the panel; closeup view of one assembled unit of the panel; stationary fan unit; front view of the rotating fan unit with fins; rear view of the rotating fan unit with fins

Fig. 5. (a)-(b) Different configurations of *Smorphacade* panels mounted on the aeroelastic models, (c) Views of a typical *Smorphacade* panel and its components.

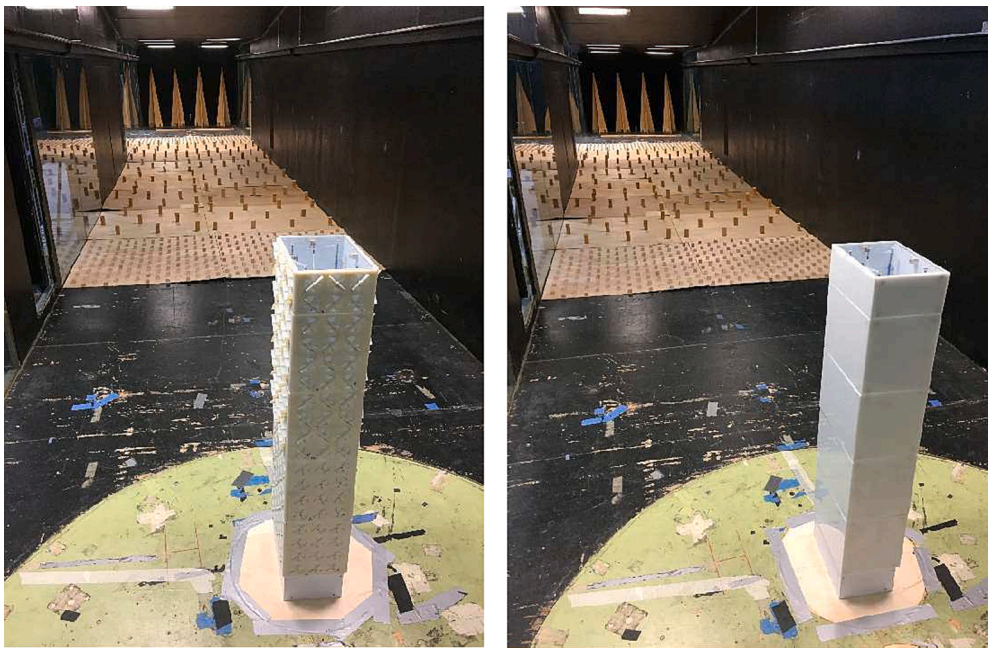

Fig. 6. The aeroelastic model with *Smorphacade* panels (left) and *dummy* panels (right) tested in the ABL section of the AABL Wind and Gust Tunnel at ISU.

flow in front of the model. A Cobra Probe (an anemometer from TFI®, Turbulent Flow Instrumentation) was used to obtain the characteristics of the incoming wind flow. Wind speed was measured at the centerline of the wind tunnel (or model), just upstream of the model, at different heights ranging from 88.9 mm (3.5 in.) to 1143 mm (45 in.). For each measurement, time histories of the wind were recorded for a duration of 60 s at a sampling frequency of 1250 Hz. The distribution of mean wind speed along height is plotted in Fig. 7, where U is the measured mean wind speed, U_H is the mean wind speed at building height (z_H), and z is the elevation above the wind tunnel floor. A power-law curve was employed to fit the measured mean wind speed along the height. The exponent of the fitted power-law function (α) was found to be 0.37, very close to the value (0.35) suggested by Architectural Institute of Japan (AIJ) [36] to represent a dense suburban/urban terrain. In addition to mean wind speeds, the longitudinal turbulence intensity of the wind ($=\sigma_u(z)*100/U(z)$) were obtained from the measurement and its vertical profile was compared with those recommended by AIJ, as shown in Fig. 7.

Both the mean velocity profile and longitudinal turbulence intensity profile in Fig. 7 show that there might be some change in the nature or trend of the boundary layer profile at z/H = 1 which implies that model roof height might be just at the boundary of the inertial sublayer or slightly outside. This is the outcome of a relatively large-scale model that was required in this study, given that the model height (H = 1.05 m) is 47.5 % of the wind tunnel test section height (2.21 m). Since this is a comparative study of the building responses between the original building without any mitigation measures and the one with the mitigation measures, this slight deviation in the input wind profile right around the building height should not affect the outcome of this study.

In addition to mean wind speed and turbulence intensity, power spectral density (PSD) is another important feature of boundary layer wind. Tieleman Spectra [37], an empirical spectra proposed for design purposes, can be expressed as.

$$\frac{nS_{uu}(z,n)}{\sigma_u^2} = \frac{20.53f_z}{1+475.1f_z^{5/3}} \tag{3}$$

$$\frac{nS_{vv}(z,n)}{\sigma_v^2} = \frac{6.83f_z}{1+75.84f_z^{5/3}} \tag{4}$$

$$\frac{nS_{ww}(z,n)}{\sigma_w^2} = \frac{1.67f_z}{1+7.23f_z^{5/3}} \tag{5}$$

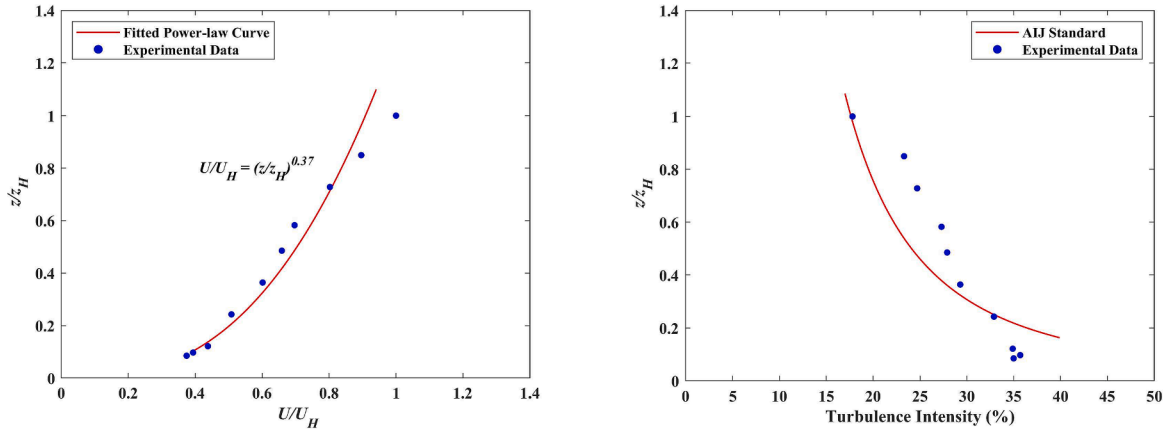

Fig. 7. Measured mean wind speed and longitudinal turbulence intensity profiles of the ABL wind.

where S_{uu}, S_{vv}, S_{ww} are power spectra of u, v and w, respectively; $f_z = \frac{nz}{U}$ is a non-dimensional variable; n is the frequency in Hz.

Comparison of PSD of along-wind, across-wind and vertical wind-speed fluctuation components u, v and w measured at the roof height (H) of the model with Tieleman Spectra shows reasonable agreement, as shown in Fig. 8.

4.2. Wind-induced dynamic response

Free vibration tests were carried out on the aeroelastic model to identify its mechanical damping and natural frequencies along each of the three DOFs at zero wind speed. Initial displacements were imposed then released one at a time at the top of the aeroelastic model in the x_b-, y_b- and α-directions, and the time histories of decaying response in these three directions were recorded using the accelerometers. A Butterworth low-pass filter was designed to remove both the noise and the contributions from higher mode shapes to ensure that each filtered signal was purely from the first mode of vibration in each given direction. The log-decrement method was used to extract the mechanical damping ratio of the aeroelastic model in x_b-, y_b- and α-directions from the filtered signals, each filtered signal was transformed into the frequency domain using Fast Fourier Transform (FFT) function. and the natural frequencies of the model were obtained by locating frequency-domain peak values. Different initial displacements were applied to the aeroelastic model, and consistency in the identified modal parameters was observed regardless of the initial displacement, showing the linearity of the aeroelastic model properties.

The modal parameters identified from the aeroelastic model equipped with *Smorphacade* and *dummy (flat) facade* are listed in Table 2 along with those of the full-scale building [30]. The similarity of the two model values will ensure that any difference observed from their wind-induced response is a result of the introduction of the *Smorphacade* and not because of the modal parameters.

The aeroelastic model was subsequently tested at wind speeds, U_H, ranging from 1.43 m/s to 5.4 m/s (Re = 2.0 x10^4 to 7.7 x10^4, based on $D_c = \sqrt{BD} = 0.213$ m), equivalent to 30.7 m/s and 116 m/s mean wind speed at building roof-height (182.9 m) in full scale, respectively, based on a reduced-velocity (RV) scale of 1. At each wind speed, time histories of the acceleration response at the roof height of the building model (H) were measured at a sampling frequency of 100 Hz for a duration of 60 s, and this was repeated three times. Accelerations in x_b-, y_b- and α-directions were calculated using Eqns. to by averaging the three records for each wind speed. The experiment was repeated for three critical angles of attack, viz., AOA = 0° (wind normal to D), 34° (wind along diagonal), and 90° (wind normal to B), for the aeroelastic model with *Smorphacade* and *Dummy facade*.

The standard deviation or RMS (root mean square) of measured accelerations (zero-mean) at roof-height of the building model in x_b-, y_b- and α-directions normalized by $n_{xb}^2 D_c$, $n_{yb}^2 D_c$ and $n_\alpha^2 D_c$, respectively, where n_{xb}, n_{yb} and n_α are the natural frequencies of the model, are given in Table 2. The normalized accelerations as a function of reduced velocity (considering n_1 = 1.63 Hz and 1.67 Hz as the first natural

Table 2
Comparison of modal parameters for aeroelastic model mounted with *Smorphacade* and *Dummy facade*.

	Damping Ratios (%)			Natural Frequency (Hz)		
Description/Direction	x_b	y_b	α	x_b	y_b	α
Model: Smorphacade	1.03	1.35	1.28	1.73	1.63	1.93
Model: Dummy facade	0.86	1.26	1.25	1.73	1.67	1.97
Full-scale Bldg.	1.00	1.00	NA	0.20	0.20	NA

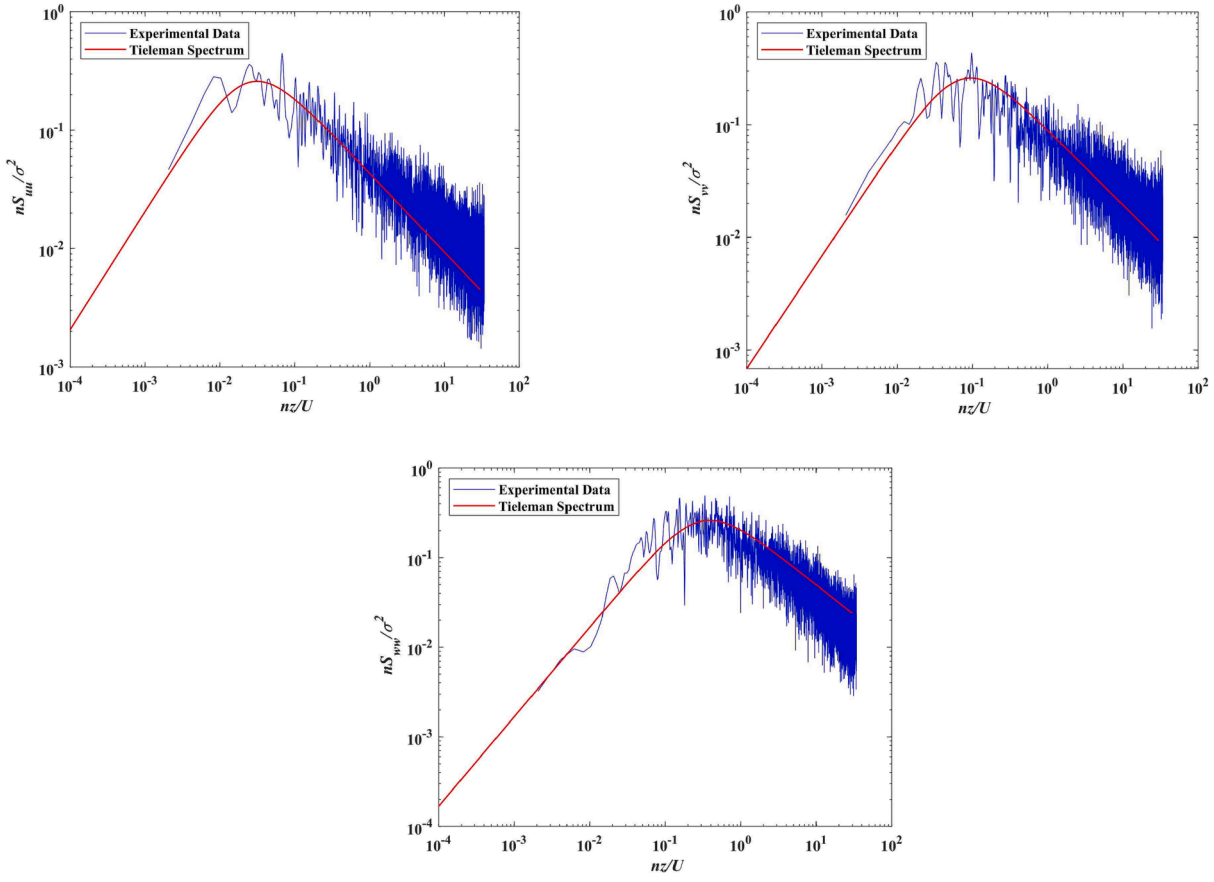

Fig. 8. PSD of wind fluctuation components u, v, w and their comparison with Tieleman Spectra.

frequency of the model with *smorphacade* and *without smorphacade*, respectively) corresponding to each of the three angles of attack are given in Figs. 9-11.

The average of the three values of RMS estimated from the three separate time history records of the acceleration response, each of 60-*sec* duration, was used here. These three 60-*sec* data records were sampled in a sequence at an interval of about 15–20 s from a continuous time history of the model response at a given wind speed. Thus, the average RMS of the three records represents that of a 180-*sec* long record, assuming its statistical stationarity which was verified by comparing the RMS of each of the three 60-*sec* records. The 180-*sec* long record in model scale represents 1465.2 *sec* or 24.4 min long record in full scale based on the time scale (1/8.14) between the model building and full-scale building, which is considered adequate for estimating statistics of a buffeting response of a structure because it is greater than 10 min duration.

The goal of this study was to measure the effectiveness of the *smorphacade* in alleviating the buffeting response of a tall building in the presence of aeroelastic effects. Its effectiveness to reduce the vortex induced vibration (VIV) response of the building was not verified. The VIV based on the rigid section model study of the building occurs at specific wind speeds (lock-in speeds) of 4.46 m/s, 2.74 m/s and 3.85 m/s for the three angles of attack, 0°, 34°, 90°, respectively, as used here. The wind speed at which the model response was measured was not set equal to the VIV wind speed or its vicinity that was necessary for observing the large-amplitude motion associated with VIV in the original or modified model. However, it can be expected that the *smorphacade* mitigation device will also help to damp the VIV response for the same reasons that was given earlier (in Section 2.2) for this device to be effective in reducing the buffeting response.

It can be seen in Figs. 9 through 11 that the proposed *Smorphacade* can reduce the wind-induced vibration for most configurations or cases (as listed in Table 1). In most cases, the effectiveness of *Smorphacade* was found to be dependent on both its configuration and the wind speed.

To quantify the effectiveness of the *Smorphacade*, parameter e was defined as follows:

$$e = \frac{1}{N}\sum_{i=1}^{N}\frac{a_{i,Dummy} - a_{i,SMF}}{a_{i,Dummy}} \times 100\% \tag{6}$$

where N is the total number of wind speeds at which the acceleration was measured, $a_{i,SMF}$ is the normalized RMS acceleration of the building model with a specific *Smorphacade* configuration under i^{th} wind speed, and $a_{i,Dummy}$ is the normalized RMS acceleration of the building model with the *dummy flat facades* and e is the *percentage reduction* in RMS acceleration.

The effectiveness e for each *Smorphacade* configuration in the three vibration directions corresponding to each of the three AOAs is summarized in Table 3, where a larger value indicates a larger reduction in RMS acceleration.

Based on the average reduction of vibration over all wind speeds, the most significant reduction (45.8 %) in vibration is observed in the α-direction when the angle of attack is 0° (normal to short-side), while the least significant reduction (13.2 %) in vibration is observed in the x_b-direction when the angle of attack is 34° (along-diagonal wind) for the best-performing *Smorphacade* configuration. It can also be concluded from the measurements that, excluding one out of the ten configurations tested at each angle of attack, the *Smorphacade* system reduced the wind-induced vibration over the entire range of wind speeds.

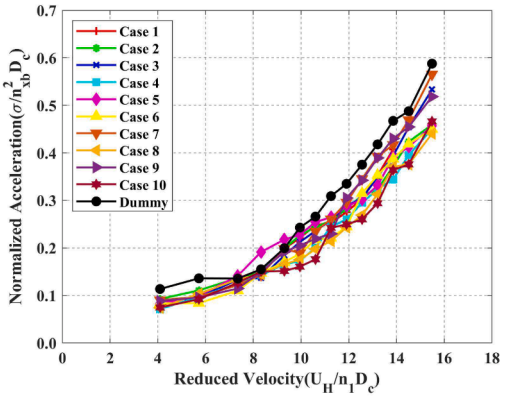

(a) Normalized RMS Acceleration in x_b-direction

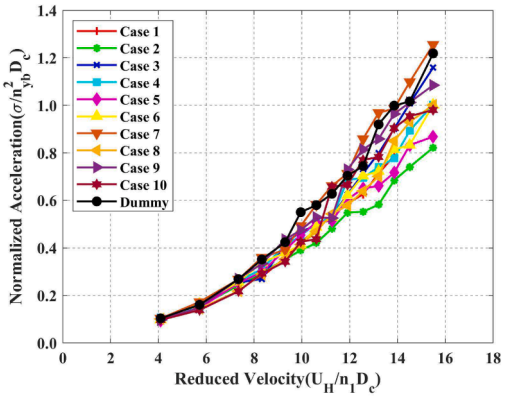

(b) Normalized RMS Acceleration in y_b-direction

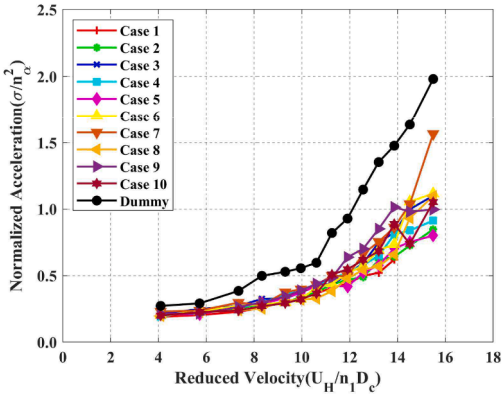

(c) Normalized RMS Acceleration in α-direction

Fig. 9. Normalized RMS Acceleration at AOA = 0°.

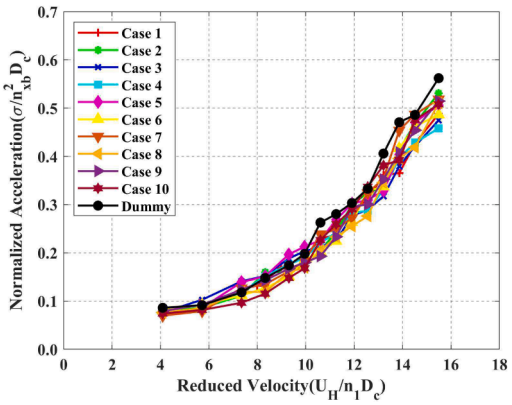

(a) Normalized RMS Acceleration in x_b-direction

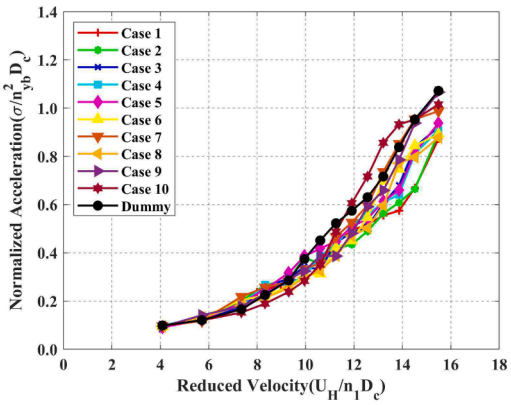

(b) Normalized RMS Acceleration in y_b-direction

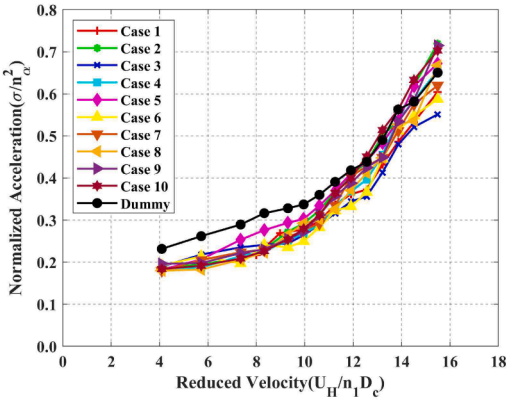

(c) Normalized RMS Acceleration in α-direction

Fig. 10. Normalized RMS Acceleration at AOA = 34°.

A study carried out by Yang et al. [28] was used to validate the results in this paper. In that study, wind tunnel tests were carried out to investigate the effects of façade-mounted vertical plates on the aerodynamic loads of tall buildings. Pressure distribution on tall buildings equipped with vertical plates were measured then used to calculate the aerodynamic forces. The comparison between Reference Model (without vertical plates) and those with vertical plates revealed that the vertical plates were very effective in reducing the wind loads. They also found vertical plates to be more effective in the across-wind direction than the along-wind direction in terms of fluctuating wind loads, and this conclusion is consistent with the results in this paper. The analysis of our results showed that the vertical fins (Configuration No. 2) can reduce wind-induced vibrations at all three angles of attack on average over all wind speeds, with the reduction greater along the across-wind direction (y_b) than along the along-wind direction (x_b). For example, at AOA = 0°, the effectiveness is 21.5 % along the y_b direction versus 13.1 % along the x_b direction. Through power spectra density analysis, the mechanism of the aerodynamic load reduction was attributed to the intensity of vortex shedding that could be attenuated by the vertical plates.

Due to limited literature in this area, results for other configurations could not be validated. However, such limitations can reflect the advantage of the *Smorphacade* presented in this paper, that is in theory able to provide an indefinite number of configurations that can be dynamically adjusted to decrease the effects of wind loads on tall buildings.

It should be noted that only accelerations were measured and used here to evaluate the relative effectiveness of vibration mitigation, whereas displacement response of a tall building plays an equally important role in determining its design performance. Failure such as cracking of façade of a building is a significant problem in buildings which occurs due to relatively large displacements. Since accelerations and displacements are related by the natural frequency of the building, the relative effectiveness of vibration mitigation for *smorphacade* configurations in terms of RMS of displacements of the building can be estimated and should not change much from those estimated with RMS of accelerations. The purpose of the present study was to study the relative performance of the *smorphacade* configurations with respect to the original building, so it refrains from estimating the absolute accelerations or displacements of a specific tall building with the same cross section as the model building because it will depend on its natural frequency, modal damping and dimensions. The natural frequencies in model scale are different from those of full scale and although RMS accelerations presented here are normalized with frequencies and characteristic dimension of the model, these normalized accelerations can be only translated to its full-scale building equivalent which has the same Scruton number (or mass-damping parameter). To find the effectiveness of a mitigation measure for tall buildings using aeroelastic models in the future, it is desirable that both displacements and accelerations are measured and the effect of Scruton number on these building responses is evaluated, to help estimate the absolute values of the responses of the full-scale building along with the relative effectiveness.

Figs. 9-11 also show that reduced velocity or wind speed could affect the effectiveness of the proposed *Smorphacade*; it can be observed from these figures that for some configurations, effectiveness is relatively small but increases as the reduced velocity increases, or vice-versa. To evaluate the performance of a *Smorphacade* configuration under different reduced velocities, the entire reduced-velocity range was divided into three segments: low, medium, and high (ranging from 4 to 9.5, 9.5 to 13, and 13 to 16, respectively). The effectiveness of all

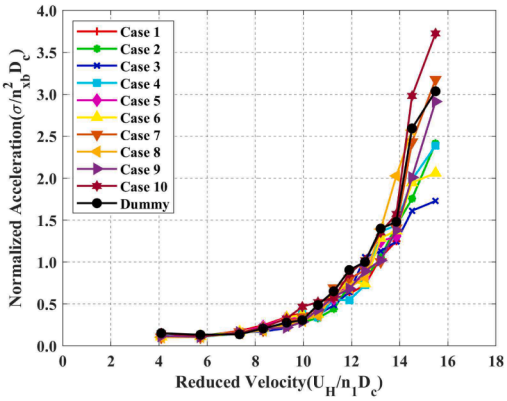

(a) Normalized RMS Acceleration in x_b-direction

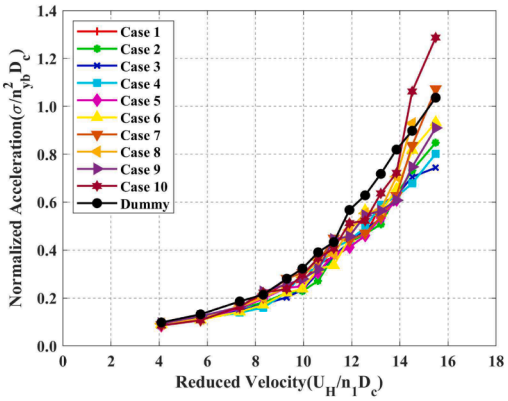

(b) Normalized RMS Acceleration in y_b-direction

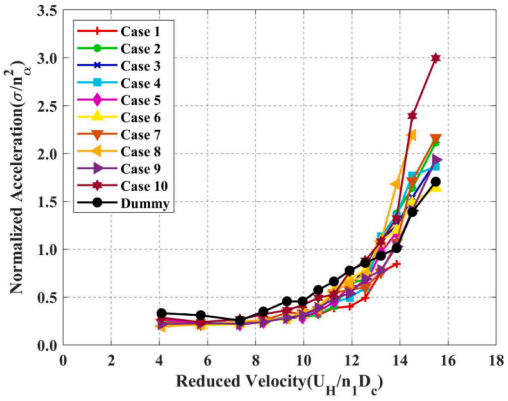

(c) Normalized RMS Acceleration in α-direction

Fig. 11. Normalized RMS Acceleration at AOA = 90°.

configurations was recalculated for those three ranges using Eqn. (6), and their values are given and compared in Table 3.

It can be observed from Table 3 that at AOA = 0°, although the best configurations in those three ranges are slightly different from those over the entire range, the difference is negligible, particularly in the x_b and α directions. The most significant difference was observed in the y_b-direction at low RV, where the best configuration is #10 (15.1 %), compared to #2 over the entire range (21.5 %), and their difference at low RV is 6.1 % (9.0 % for Config. 2). For AOA = 34°, there is a large difference between the overall best configuration and the best configuration at low reduced velocity, especially in the y_b-direction, Configuration #1 is the best configuration for the entire range (14.2 %), although it could even amplify the wind-induced vibration at low reduced velocities (-3.3 %). Configuration #8 and #3 are the best overall configurations in the x_b and α directions, respectively, but they do not perform as well at low reduced velocities; there are big differences with the best configurations in this range. For AOA = 90°, the best configurations at each reduced velocity range are slightly different from those over the entire range, although the differences are small. It should be noted for this AOA that all configurations except Configuration #1 failed to reduce wind-induced vibration in the α-direction at high reduced velocities. For most cases, the capability for controlling the wind-induced vibration generally increases with reduced velocity, as can be concluded from Table 3.

Average effectiveness values of each configuration of the *Smorphacade* in specific directions and all three directions combined, across all three angles of attack and over the full range of reduced velocities, are tabulated in Table 4. The table shows that the best effectiveness was accomplished by Configuration 4 for x_b (15 %), Configuration 2 for y_b (17.1 %), Configuration 1 for α (31.3 %), and Configuration 1 (18.6 %) for all three directions combined.

The above analysis shows that one can devise a strategy to modify the *Smorphacade* to take on a particular configuration depending on the direction of critical vibration to be controlled over a range of wind speeds and wind directions.

4.3. Static tests for mean loads

Static tests on section models with selected configurations (Fig. 12) of the *smorphacade* and the one without it (bare model) were conducted to obtain their static aerodynamic load coefficients for comparison of their estimated mean responses. All selected configurations, based on their effectiveness to reduce vibrations, were tested for all three angles of attack except Config. 10 which was tested only for AOA of 0^0 because it was amongst the top four configurations in effectiveness only for this AOA. The dimensions of the section model without the *smorphacade* panels were: B = 258 mm (10.22 in), D = 172 mm (6.81in), $D_c=\sqrt{BD}$ = 211 mm (8.29 in), L = Length = 417.5 mm (16.44 in); B/D = 1.5, L/D = 2.4. The dimensions B and D for the section model with the *smorphacade* panels were larger by 16 mm because of the panel thickness of 6 mm and a gap of 2 mm behind the panels: B = 274 mm (10.79 in), D = 188 mm (7.40 in), $D_c=\sqrt{BD}$ = 227 mm (8.94 in). The section model was mounted vertically on a JR3 six-component force sensor fixed to the floor of the wind tunnel, and mean drag, lift and torsional loads were measured under an uniform and smooth flow condition (uniform wind speed profile with < 0.2 % turbulence intensity) at three angles of attack: 0, 34 and 90 deg. Two runs of 30-*sec* at 100 Hz were recorded at each of the two wind speeds (U), 6.1 m/s (20.1 ft/s) and 10.2 m/s (33.4 ft/s), and the average of normalized loads or load coefficients for drag (C_D), lift (C_L) and torsion (C_M) were calculated from the four records as follows: $C_D = \frac{F_D}{\frac{1}{2}\rho U^2 D_c L}$, $C_L = \frac{F_L}{\frac{1}{2}\rho U^2 D_c L}$, $C_M = \frac{M}{\frac{1}{2}\rho U^2 D_c^2 L}$, as tabulated in Table 5. The

Table 3
Effectiveness (e) of *Smorphacade* configurations for each direction and RV range.

AOA	Config. No.	Average over All RVs			Low RV			Medium RV			High RV			Avg
		Direction			Direction			Direction			Direction			All Dirs.
		x_b	y_b	α	x_b	y_b	α	x_b	y_b	α	x_b	y_b	α	
0°	1	13.4	14.7	**45.8**	12.2	9.0	38.2	14.2	17.5	47.9	14.3	21.7	**59.7**	24.6
	2	13.1	**21.5**	44.1	8.0	9.0	32.6	12.9	25.5	46.1	19.6	**32.0**	56.0	26.2
	3	14.0	8.9	36.5	15.1	7.1	27.6	14.6	11.9	40.1	12.0	7.2	43.1	19.8
	4	22.0	10.6	39.1	19.8	4.1	30.6	23.6	11.2	39.0	22.8	17.9	50.0	23.9
	5	10.7	16.0	43.2	3.4	9.3	32.3	11.7	15.0	44.1	18.7	25.8	55.8	23.3
	6	20.4	12.3	39.5	20.7	4.5	32.3	22.5	14.8	42.8	17.6	19.0	44.5	24.1
	7	11.5	-2.0	32.7	13.4	-0.3	26.0	13.8	-2.4	36.9	6.1	-3.8	35.8	14.1
	8	22.6	15.7	44.3	16.7	13.0	35.5	28.0	17.9	48.4	23.4	16.3	50.2	**27.5**
	9	13.2	4.5	34.3	14.9	3.1	30.8	15.3	5.1	33.5	8.4	5.4	39.5	17.3
	10	**24.4**	12.2	41.1	20.0	15.1	35.6	**29.1**	8.9	41.2	23.9	12.5	47.8	25.9
34°	1	9.1	**14.2**	15.9	2.4	-3.3	24.0	8.7	15.6	15.5	14.6	**25.6**	10.2	13.1
	2	7.9	10.0	9.7	3.8	-8.4	23.5	10.5	17.4	6.5	9.6	23.9	-3.6	9.2
	3	6.9	8.9	**18.3**	-6.3	-4.3	20.6	11.6	17.1	19.4	**17.5**	15.1	14.0	11.4
	4	9.6	7.6	15.3	3.1	-6.8	25.3	10.9	14.5	15.3	16.1	17.1	2.6	10.8
	5	3.9	5.5	7.0	-2.0	-6.1	15.6	3.6	8.9	4.8	11.6	15.6	-0.9	5.5
	6	10.6	9.1	18.2	7.6	-3.6	23.9	12.8	20.7	20.4	11.7	10.4	8.4	12.6
	7	7.6	1.4	14.0	8.3	-8.0	23.0	8.2	11.3	11.5	6.0	0.8	5.9	7.7
	8	**13.2**	12.4	15.3	9.0	0.2	**26.0**	17.2	22.5	12.7	13.4	14.8	5.0	**13.6**
	9	8.3	4.9	11.9	1.9	-4.7	22.5	13.0	15.2	10.3	10.4	4.1	0.8	8.4
	10	11.0	3.7	10.2	16.0	8.7	25.3	7.9	6.8	7.7	8.6	-6.4	-5.4	8.3
90°	1	6.6	15.2	**32.1**	-5.7	8.8	28.1	13.5	19.5	**42.0**	20.0	20.5	17.5	**18.0**
	2	15.7	19.8	14.0	5.2	13.2	25.4	22.6	24.4	31.7	20.0	22.3	-22.2	16.5
	3	**17.9**	**21.0**	14.5	12.8	17.2	26.4	14.1	21.8	27.1	**29.0**	24.8	-16.1	17.8
	4	13.5	18.3	13.9	9.9	19.0	24.1	17.9	14.5	33.4	12.6	22.2	-23.0	15.2
	5	6.4	19.0	22.4	-1.3	13.2	26.4	12.3	22.1	31.3	11.3	**25.6**	-10.1	15.9
	6	8.5	17.7	14.8	-0.6	17.9	29.8	10.0	19.4	19.2	18.1	15.4	-9.5	13.7
	7	7.1	11.2	15.6	7.6	8.9	23.8	5.2	12.0	27.4	8.7	13.0	-9.4	11.3
	8	8.2	10.7	8.2	13.0	10.0	28.2	15.5	11.5	21.2	-11.9	10.3	-46.7	9.0
	9	12.4	11.6	20.4	9.8	5.0	28.9	12.8	12.3	28.3	15.1	19.0	0.0	14.8
	10	-7.5	6.0	-6.6	-4.2	11.1	12.1	-8.8	9.4	8.4	-10.2	-4.8	-48.7	2.7

most effective configuration of the *Smorphacade* in a specific direction corresponding to each AOA is marked in bold font.

denotes best configuration at that specific range of RV

yy.y denotes best configuration at that specific range of RV and the maximum effectiveness in a specific direction across all RVs

Table 4
The averaged effectiveness (e) of *Smorphacade* across all three AOAs and/or all three directions.

Smorphacade Configuration No.	Average across all three AOAs in specific directions			Average of all three AOAs across all three directions
	x_b	y_b	α	
1	9.7	14.7	**31.3**	**18.6**
2	12.2	**17.1**	22.6	17.3
3	12.9	12.9	23.1	16.3
4	**15.0**	12.2	22.8	16.7
5	7.0	13.5	24.2	14.9
6	13.2	13.0	24.2	16.8
7	8.7	3.5	20.8	11.0
8	14.7	12.9	22.6	16.7
9	11.3	7.0	22.2	13.5
10	9.3	7.3	14.9	12.3

The most effective configuration of the *Smorphacade* in a specific direction across all AOAs and across all AOAs and directions is marked in bold font.

maximum error in the load coefficients was estimated to be ± 5 %.

For all selected configurations tested, when compared to the bare model without *Smorphacade*, the mean drag reduces or remains the same, the mean lift (across-wind) increases slightly but remains mostly small, while the mean torsional moment remains the same, close to zero, as shown in Table 5. The additional benefit of the *Smorphacade* in reducing the mean drag, the most significant wind load, and hence the overturning moment, in addition to the dynamic loads can thus be seen.

5. Summary

In this paper, a smart morphing façade (*Smorphacade*) was proposed and its effectiveness in mitigation of wind-induced vibration of tall buildings investigated using an aeroelastic model-testing scheme. The response of the model at three critical angles of attack (0°, 34°, and 90°) was obtained in three directions (x_b-, y_b- and α-directions) of the building. A comparison between the model equipped with *Smorphacade* and one with flat panels showed that while the proposed system can reduce wind-induced vibration of tall buildings, its efficiency is dependent on many factors such as wind speed, angle of attack, vibration direction, etc.

The following is a summary of the findings (see Tables 3-4, Figs. 13-14) for *Smorphacade* system performance with respect to mitigation of tall-building response where Table 1 defines all the *Smorphacade* configurations:

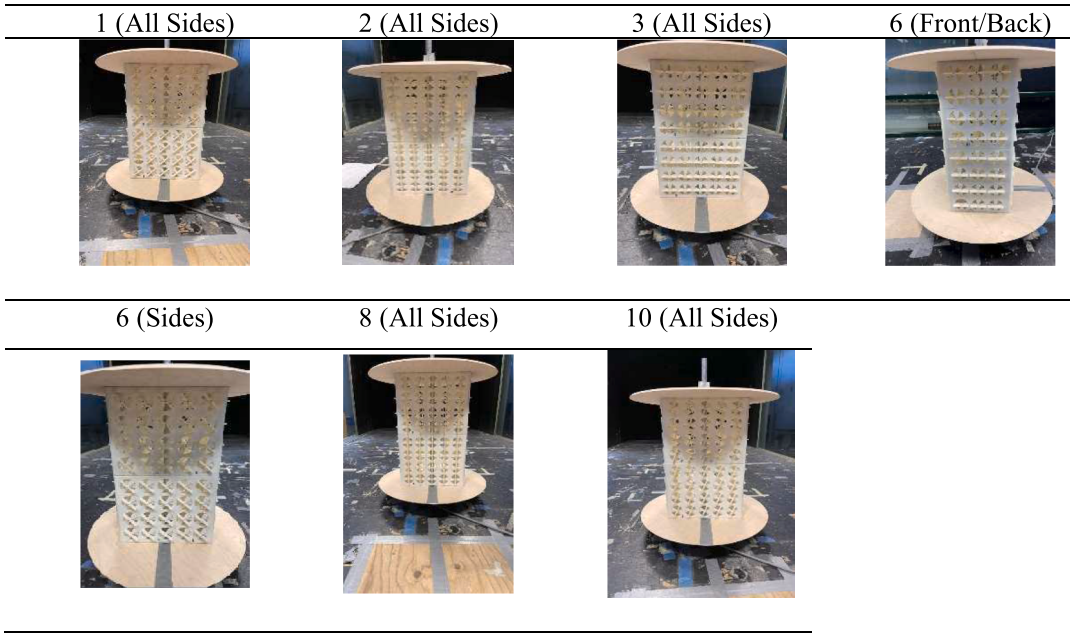

Fig. 12. Models of selected configurations tested inside the wind tunnel.

Table 5
Mean Aerodynamic Load Coefficients.

Config	AOA 0^0			AOA 34^0			AOA 90^0			
	C_D	C_L	C_M	C_D	C_L	C_M	C_D	C_L	C_M
0	1.10	−0.06	−0.02	1.44	0.42	0.03	1.73	−0.01	−0.02
1	1.03	−0.06	−0.02	1.38	0.29	0.05	1.47	−0.13	−0.02
2	0.98	−0.22	−0.05	1.37	0.28	0.05	1.49	−0.17	−0.02
3	1.08	−0.09	−0.02	1.46	0.35	0.05	1.55	−0.07	−0.02
6	1.06	−0.09	−0.02	1.42	0.27	0.04	1.49	−0.13	−0.02
8	1.03	−0.12	−0.03	1.38	0.21	0.04	1.44	−0.11	−0.02
10	0.97	−0.13	−0.03	Not Tested			Not Tested		

Note: Config. 0 is the Bare Model without *Smorphacade*.

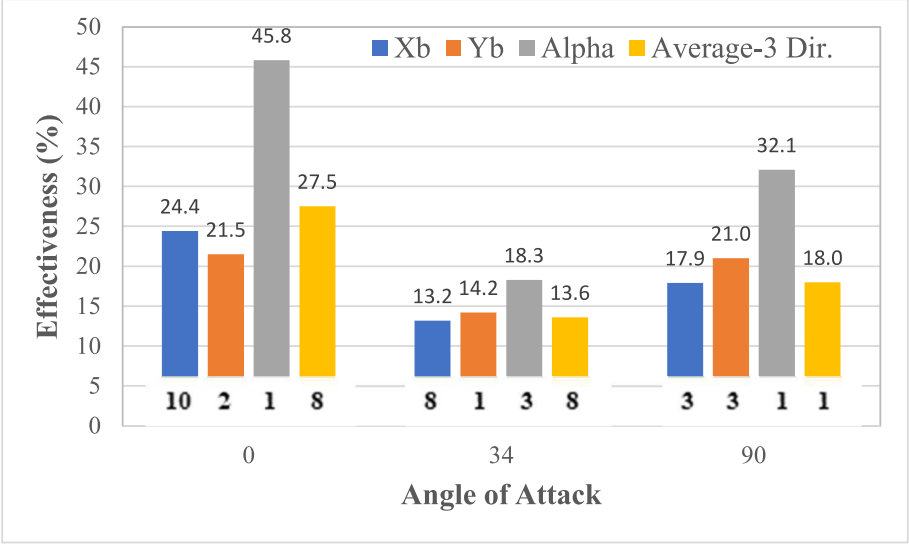

Fig. 13. Effectiveness of *Smorphacade* Configurations at different Angles of Attack.

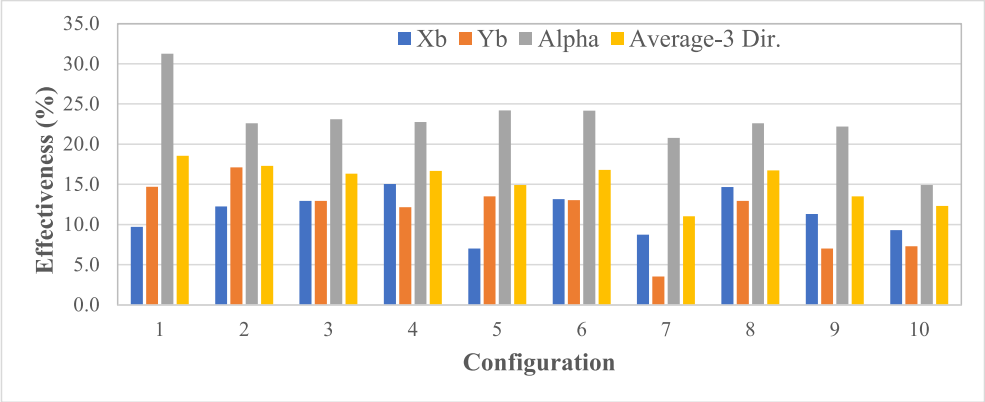

Fig. 14. The averaged effectiveness (e) of *Smorphacade* across all three AOAs and/or all three directions.

5.1. Angle of attack specific averaged over all wind speeds (Table 3, Fig. 13)

AOA = 0°.

- Configuration #10 (fins inclined at an angle of 70°), Configuration #2 (fins inclined at an angle of 90°) and Configuration #1 (fins inclined at an angle of 45°) were found to be the most effective in reducing vibration in the x_b-direction (24.4 %), y_b-direction (21.5 %) and α-direction (45.8 %), respectively, while Configuration #8 (fins inclined at angles of 0° and 90° on front/rear faces and side faces, respectively) was found to be the most effective in reducing average vibration (27.5 %) in all three directions. Configurations #8, 2, and 10 were the most effective in reducing average vibration in all three directions (27.5 %, 26.2 %, 25.9 %, respectively) in that order over the full range of wind speeds.

AOA = 34°.

- Configuration #8, Configuration #1 and Configuration #3 (fins inclined at an angle of 0°) were found to be the most effective in reducing vibration in the x_b-direction (13.2 %), y_b-direction (14.2 %) and α-direction (18.3 %), respectively, while Configuration #8 was found to be the most effective in reducing average vibration (13.6 %) in all three directions. A notable difference between performance of the *Smorphacade* system and dummy panels was observed at higher reduced velocities (RV greater than 10) in the x_b- and y_b-directions, and the performance of the *Smorphacade* system in the α-direction was found to be better at lower reduced velocities (RV < 10). Configurations #8, 1, and 6 were the most effective in reducing the average vibration in all three directions (13.6 %, 13.1 %, 12.6 %, respectively) in that order over the full range of wind speeds.

AOA = 90°.

- Configuration #3, Configuration #3 and Configuration #1 were found to be the most effective in reducing vibration in the x_b-direction (17.9 %), y_b-direction (21 %) and α-direction (32.1 %), respectively, while Configuration #1 was found to be the most effective in reducing average vibration (18 %) in all three directions. Configurations #1, 3, and 2 were the most effective in reducing the average vibration in all three directions (18 %, 17.8 %, 16.5 %, respectively) in that order over the full range of wind speeds.

5.2. High-Wind-speed specific

Vibration reductions of 17.5 to 29 %, 25.6 to 32.0 % and 14.0 to 59.7 % in the x_b-direction, y_b-direction and α-directions, respectively, can be achieved at higher wind speeds during intense windstorms, depending on the wind direction with respect to the building orientation (Table 3).

5.3. Direction of vibration specific

Configurations #4, 2, and 1 were the most effective in reducing average vibration in the x_b-direction, y_b-direction and α-directions, respectively, averaged over all three AOA and wind speeds (Table 4, Fig. 14).

5.4. Overall vibration reduction

Configurations #1, 2, 6, 8, 4 and 3 were the most effective in reducing the average vibration in all three directions combined, in that order, 18.6 %, 17.3 %, 16.8 %, 16.7 %, 16.7 %, 16.3 %, respectively, averaged over all three AOA and wind speeds (Table 4, Fig. 14).

Compared to the traditional architectural or energy savings components, this study is one-of-a-kind in providing the data required and experimentally validated justification for revisioning building facade systems as multifunctional structural units. The results show that manipulating *Smorphacade* configurations could result in decreasing potential vibrations observed for winds of different intensity under different wind directions. This perfectly justifies the community of structural engineering and architectural engineering to move from designing facades as passive elements and invest more in designing envelope components capable of responding to different wind regimes in a changing climate.

CRediT authorship contribution statement

Fangwei Hou: Methodology, Writing – original draft, Investigation, Formal analysis, Validation. **Partha P. Sarkar:** Conceptualization, Methodology, Investigation, Writing – review & editing, Supervision, Project administration, Funding acquisition. **Alice Alipour:** Conceptualization, Project administration, Funding acquisition, Writing – review & editing.

Declaration of Competing Interest

The authors declare that they have no known competing financial interests or personal relationships that could have appeared to influence the work reported in this paper.

Data availability

The authors do not have permission to share data.

Acknowledgement

This research was primarily supported by the U.S. National Science Foundation (NSF) under research grant No. NSF-CMMI- 1826356 and partially supported by State Key Laboratory for Disaster Reduction in Civil Engineering (SLDRCE), Tongji University, Shanghai, PRC under research grant No. SLDRCE17-04. Their support is gratefully acknowledged.

References

[1] Park HS, Park CL. Drift control of high-rise buildings with unit load method. Struct Des Tall Build 1997;6:23–35. https://doi.org/10.1002/(SICI)1099-1794(199703)6:1<23::AID-TAL80>3.0.CO;2-1.
[2] Park HS, Sohn HG, Kim IS, Park JH. Application of GPS to monitoring of wind-induced responses of high-rise buildings. Struct Des Tall Spec Build 2008;17:117–32. https://doi.org/10.1002/tal.335.
[3] Kwok KCS, Burton MD, Abdelrazaq AK. Wind-induced motion of tall buildings: Designing for habitability 2015. https://doi.org/10.1007/978-3-319-47548-6.
[4] Chan CM, Huang MF, Kwok KCS. Integrated wind load analysis and stiffness optimization of tall buildings with 3D modes. Eng Struct 2010;32:1252–61. https://doi.org/10.1016/j.engstruct.2010.01.001.
[5] Walton D, Lamb S, Kwok KCS. A review of two theories of motion sickness and their implications for tall building motion sway. Wind Struct An Int J 2011;14:499–515. 10.12989/was.2011.14.6.499.
[6] Micheli L, Alipour A, Laflamme S, Sarkar P. Performance-based design with life-cycle cost assessment for damping systems integrated in wind excited tall buildings. J Eng Struct 2019;195:438–51. https://doi.org/10.1016/j.engstruct.2019.04.009.
[7] Micheli L, Cao L, Laflamme S, Alipour A. Life-Cycle Cost Evaluation Strategy for High-Performance Control Systems under Uncertainties. ASCE J Eng Mech 2020;146(2):1–15. https://doi.org/10.1061/(ASCE)EM.1943-7889.0001711. 04019134.
[8] Micheli L, Hong J, Laflamme S, Alipour A. Surrogate models for high performance control systems in wind-excited tall buildings. J Appl soft Comput 2020;90:1–15. https://doi.org/10.1016/j.asoc.2020.106133. 106133.
[9] Micheli L, Alipour A, Laflamme. S. Multiple-surrogate models for probabilistic performance assessment of wind-excited tall buildings under uncertainties. ASCE-ASME J Risk Uncertain Eng Syst Part A Civ Eng 2020;6:04020042.
[10] Hareendran SP, Alipour A, Shafei B, Sarkar P. "Performance-based wind design of tall buildings considering the nonlinearity in building response", ASCE. J Struct Eng 2022.
[11] Hareendran SP, Alipour A. Prediction of nonlinear structural response under wind loads using deep learning techniques. Appl Soft Comput 2022;129:109424.
[12] Hayashida H, Mataki Y, Iwasa Y. Aerodynamic damping effects of tall building for a vortex induced vibration. J Wind Eng Ind Aerodyn 1992;43:1973–83. https://doi.org/10.1016/0167-6105(92)90621-G.
[13] Kawai H. Effect of corner modifications on aeroelastic instabilities of tall buildings. J Wind Eng Ind Aerodyn 1998;74–76:719–29. https://doi.org/10.1016/S0167-6105(98)00065-8.
[14] Kim Y-M, You K-P, Ko N-H. Across-wind responses of an aeroelastic tapered tall building. J Wind Eng Ind Aerodyn 2008;96:1307–19.
[15] Kim Y, Kanda J. Characteristics of aerodynamic forces and pressures on square plan buildings with height variations. J Wind Eng Ind Aerodyn 2010;98:449–65. https://doi.org/10.1016/j.jweia.2010.02.004.
[16] Tanaka H, Tamura Y, Ohtake K, Nakai M, Kim YC. Experimental investigation of aerodynamic forces and wind pressures acting on tall buildings with various unconventional configurations. J Wind Eng Ind Aerodyn 2012;107–108:179–91.
[17] Tamura T, Miyagi T, Kitagishi T. Numerical prediction of unsteady pressures on a square cylinder with various corner shapes. J Wind Eng Ind Aerodyn 1998;74–76:531–42.
[18] Bairagi AK, Dalui SK. Comparison of aerodynamic coefficients of setback tall buildings due to wind load. Asian J Civ Eng 2018;19:205–21.
[19] Chakraborty S, Dalui SK, Ahuja AK. Wind load on irregular plan shaped tall building - A case study. Wind Struct 2014;19:59–73.
[20] Zahid Iqbal QM, Chan ALS. Pedestrian level wind environment assessment around group of high-rise cross-shaped buildings: Effect of building shape, separation and orientation. Build Environ 2016;101:45–63.
[21] van Moeseke G, Gratia E, Reiter S, De Herde A. Wind pressure distribution influence on natural ventilation for different incidences and environment densities. Energy Build 2005;37:878–89.
[22] Lou W, Huang M, Zhang M, Lin N. Experimental and zonal modeling for wind pressures on double-skin facades of a tall building. Energy Build 2012;54:179–91.
[23] Hassanli S, Hu G, Kwok KCS, Fletcher DF. Utilizing cavity flow within double skin façade for wind energy harvesting in buildings. J Wind Eng Ind Aerodyn 2017;167:114–27.
[24] Hassanli S, Hu G, Fletcher DF, Kwok KCS. Potential application of double skin façade incorporating aerodynamic modifications for wind energy harvesting. J Wind Eng Ind Aerodyn 2018;174:269–80.
[25] Marques da Silva F, Glória GM. Gap inner pressures in multi-storey double skin facades. Energy Build 2008;40:1553–9.
[26] Hu G, Hassanli S, Kwok KCS, Tse KT. Wind-induced responses of a tall building with a double-skin façade system. J Wind Eng Ind Aerodyn 2017;168:91–100.
[27] Fu, TS, Johnson, EA. Control strategies for a distributed mass damper system. Proceedings of the American Control Conference, St. Louis, MO, USA, June 10-12, 2009 (pp. 3921-3925), 10.1109/ACC.2009.5160718.
[28] Yuan K, Hui Y, Chen Z. Effects of facade appurtenances on the local pressure of high-rise building. J Wind Eng Ind Aerodyn 2018;178:26–37.
[29] Yang Q, Liu Z, Hui Y, Li Z. Modification of aerodynamic force characteristics on high-rise buildings with arrangement of vertical plates. J Wind Eng Ind Aerodyn 2020;200:104155.
[30] Pomaranzi G, Daniotti N, Schito P, Rosa L, Zasso A. Experimental assessment of the effects of a porous double skin façade system on cladding loads. J Wind Eng Ind Aerodyn 2020;196:104019.
[31] Jafari M, Alipour A. Review of approaches, opportunities, and future directions for improving aerodynamics of tall buildings with smart facades. J Sustainable Cities and Society 2021;72(102979):1–20.
[32] Jafari M, Alipour A. Aerodynamic shape optimization of rectangular and elliptical double-skin façades to mitigate wind-induced effects on tall buildings. J Wind Eng Ind Aerodyn 2021;213(104586):1–25.
[33] Abdelaziz K, Alipour A, Hobeck J. A smart façade system controller for optimized wind-induced vibration mitigation in tall buildings. J Wind Eng Ind Aerodyn 2021;212(104601):1–10.
[34] Melbourne WH. Comparison of measurements on the CAARC standard tall building model in simulated model wind flows. J Wind Eng Ind Aerodyn 1980. https://doi.org/10.1016/0167-6105(80)90023-9.
[35] Hou F, Sarkar PP. Aeroelastic model tests to study tall building vibration in boundary-layer and tornado winds. Eng Struct 2020;207:110259.
[36] Architectural Institute of Japan (AIJ). AIJ recommendations for loads on buildings. Architectural Institute of Japan; 1996.
[37] Tieleman HW. Universality of velocity spectra. J Wind Eng Ind Aerodyn 1995;56:55–69.